Concentric-shell algorithm for Auger and core-level photoelectron diffraction: Theory and applications

D. K. Saldin, G. R. Harp,* and X. Chen

Department of Physics and Laboratory for Surface Studies, University of Wisconsin-Milwaukee,
1900 E. Kenwood Boulevard, Milwaukee, Wisconsin 53201
(Received 22 March 1993)

A full multiple-scattering method is described for the calculation of angle-resolved photoelectron, Auger-electron, and Kikuchi-electron diffraction patterns. The method is particularly useful for the range of electron kinetic energies from about 50 eV to a few thousand eV. Approximations that take advantage of the finite experimental angular resolution, and, for the higher electron kinetic energies, the dominant electron forward scattering, are implemented, and may be used to improve computational efficiency. Comparisons of calculations with an experimental *LVV* Auger diffraction pattern from a Cu(001) surface show excellent agreement. The simulated diffraction patterns are also used to investigate the effects of holographic reconstruction in the case of the adsorbate system O/Ni(001), where we examine the influence of multiple scattering. In the case of the Cu(001) diffraction pattern, we examine the effects of the thickness of a film on holographic reconstruction.

I. INTRODUCTION

In recent years, angle-resolved diffuse electron diffraction (including x-ray photoelectron diffraction, Auger-electron diffraction, and Kikuchi-electron diffraction) has contributed much to the understanding of the growth characteristics of films prepared by molecular-beam epitaxy.[1] The structural information obtained by the use of diffuse electron diffraction has played a key role in the understanding of important electronic and magnetic properties, such as, e.g., giant magnetoresistance in Co/Cu(111) superlattices.[2] In recent years, it has been suggested[3-5] that the principles of holography[6,7] may be used to reconstruct three-dimensional representations of the relative positions of atoms near a surface from the information on a diffuse electron-diffraction pattern. The essential features of this idea have now been demonstrated experimentally by a number of groups.[8-12]

Advancement of these fields would be greatly aided by the development of efficient methods for the simulating diffuse electron-diffraction patterns by computer. Such simulations are useful in two ways: (1) they provide comparisons to experimental data, allowing the extraction of maximal information from a given measurement, and (2) they enable rapid testing of proposed data-analysis techniques on large bodies of data, sometimes even providing data which, although physically meaningful, are not available in a real-world experiment.

Diffuse electron-diffraction patterns are formed when electrons are emitted from atoms near the surface of a crystal by, e.g., a photoemission or Auger emission process. If the kinetic energies of these electrons lie in the medium-energy range (~300 to a few 1000 eV), characteristic peaks along low Miller index directions arise on these diffraction patterns. Such peaks provide convenient "fingerprints" of the crystal structure and orientation.[13-17,1] However, subtle structural information regarding, e.g., tetragonal strain, requires comparison of such diffraction patterns with simulations. At the same time, diffuse electron-diffraction patterns with electron kinetic energy below ~300 eV admit no simple interpretation, and always require comparison with simulations as part of the data analysis. In general, these simulations require a sophisticated multiple-scattering theory.

In this paper we describe an accurate and efficient multiple-scattering scheme for the calculation of such diffraction patterns, which may offer some unique advantages over prior methods. Our method is based on a cluster model in which the atoms surrounding each emitter are subdivided into a series of concentric shells, which allows a convenient classification of the multiple scattering into intrashell and intershell processes. Such a scheme was first applied to the calculation of x-ray-absorption near-edge structure (XANES),[18,19] and subsequently adapted from the calculation of low-energy electron-diffraction (LEED) intensities.[20,21] In our present paper we describe an extension of the scheme for the calculation of photoelectron, Auger, and Kikuchi diffraction.

II. MULTIPLE-SCATTERING THEORY

The history of multiple-scattering calculations for angle-resolved photoemission can be traced at least as far back as the work of Liebsch,[22] who treated emission from an adsorbate on a surface. Pendry[23] proposed a theory for angle-resolved valence-band photoemission and Tong and co-workers[24-26] proposed a corresponding treatment for photoemission from molecular orbitals and atomic core states. All these schemes rely on the computational machinery of low-energy electron-diffraction (LEED) theory for evaluating the multiple electron scattering in ordered atomic layers. The other major class of techniques relies on the short inelastic-scattering length of

low- and medium-energy electrons in solids to restrict the multiple scattering of the photoelectrons to a cluster of atoms localized around the photoemitter. The advantage of such a technique is the relaxation of the requirement of translational symmetry in the layers of atoms parallel to the surface. Such cluster techniques have been developed by Barton and co-workers,[27,28] Fritzsche,[29] and Friedman and Fadley.[30] In such schemes all the interatom propagation of the electrons is represented by Green's functions which relate the amplitudes of a spherical-wave expansion of the wave field about a particular atom to those of the same wave field about another. The evaluation of these Green's functions turns out to be the limiting factor in the speed of such calculations. Therefore, fast approximate schemes such as the Taylor-series magnetic quantum number expansion (TS-MQNE),[27] the reduced angular momentum expansion (RAME),[29] and the separable Green's functions of Rehr and Albers[31,30] have been employed to speed up the calculations.

We describe here the application to Auger and photoelectron diffraction of an *exact* multiple-scattering cluster scheme, based on the classification of the cluster into a series of concentric shells, centered on the electron emitter, and containing atoms of approximately the same distance from the emitter. Such a scheme had been earlier proposed for LEED by Pendry[20] and implemented by Saldin and Pendry.[21] The idea was to overcome the disastrous N^3 scaling of computer time of traditional layer methods, where N is the number of atoms per two-dimensional unit cell in each layer.

When an atom emits an electron by an Auger or photoemission process, the resulting wave field could be written as the following linear combination, with amplitudes $A_L^{(0)}$, of outgoing spherical waves:

$$\sum_L A_L^{(0)} h_l^{(1)}(kr) Y_L(\hat{\mathbf{r}}) , \tag{1}$$

where $(lm) \equiv L$ are angular momentum quantum numbers, $\mathbf{r}$ is a position vector with respect to an origin at the emitter, k is the wave number of the emitted electrons, $h_l^{(1)}$ is a Hankel function of order l, and Y_L is a spherical harmonic. The extent of the propagation of such a wave through a material will depend on the fairly short inelastic-scattering length, and hence be restricted to a localized cluster of atoms surrounding the emitter. For computational convenience we divide the cluster into a series of N concentric shells centered on the emitter. We also suppose that the total electron wave field between the qth and the $(q+1)$th shells takes the same form as (1), but with expansion coefficients $A_L^{(q)}$, which we collectively represent by the vector $\mathbf{A}^{(q)}$. Thus the task of determining the electron wave field emerging to some external detector after multiple scattering with all atoms of the cluster is effectively one of evaluating the vector $\mathbf{A}^{(N)}$, representing the corresponding expansion coefficients of the wave field propagating outwards from the Nth shell.

The elements of the vector $\mathbf{A}^{(N)}$ may be computed from known values of $\mathbf{A}^{(0)}$ by the following algorithm:[20,21]

$$\mathbf{A}^{(N)} = \mathbf{A}^{(0)} \mathbf{S}^{(N)} , \tag{2}$$

where the matrix $\mathbf{S}^{(N)}$ may be evaluated by the following pair of coupled recursion relations:

$$\mathbf{S}^{(q+1)} = \mathbf{S}^{(q)} (\mathbf{I} - \mathbf{T}_{q+1}^{OI} \mathbf{J}_q^{IO})^{-1} (\mathbf{I} + \mathbf{T}_{q+1}^{OO}) \tag{3}$$

and

$$\mathbf{J}_{q+1}^{IO} = \mathbf{T}_{q+1}^{IO} + (\mathbf{I} + \mathbf{T}_{q+1}^{II}) \mathbf{J}_q^{IO} (\mathbf{I} - \mathbf{T}_{q+1}^{OI} \mathbf{J}_q^{IO})^{-1} (\mathbf{I} + \mathbf{T}_{q+1}^{OO}) \tag{4}$$

with the starting conditions

$$\mathbf{S}^{(0)} = \mathbf{I} \tag{5}$$

and

$$\mathbf{J}_0^{IO} = \mathbf{t}_c , \tag{6}$$

where $\mathbf{t}_c$ is the t matrix of the emitter atom.

In the above expressions, $\mathbf{I}$ is a unit matrix, and the elements, T_q^{OO}, T_q^{OI}, T_q^{II}, and T_q^{IO}, of the scattering matrices of the qth shell are given by

$$T_{qLL'}^{OO} = \sum_{iL_i} \sum_{jL_j} g_{LL_i}^{oi} T_{L_iL_j}^{ij} \tilde{g}_{L_jL'}^{jo} , \tag{7}$$

$$T_{qLL'}^{OI} = \sum_{iL_i} \sum_{jL_j} g_{LL_i}^{oi} T_{L_iL_j}^{ij} g_{L_jL'}^{jo} , \tag{8}$$

$$T_{qLL'}^{II} = \sum_{iL_i} \sum_{jL_j} \tilde{g}_{LL_i}^{oi} T_{L_iL_j}^{ij} g_{L_jL'}^{jo} , \tag{9}$$

and

$$T_{qLL'}^{IO} = \sum_{iL_i} \sum_{jL_j} \tilde{g}_{LL_i}^{oi} T_{L_iL_j}^{ij} \tilde{g}_{L_jL'}^{jo} , \tag{10}$$

where

$$g_{LL'}^{ij} = 4\pi(1-\delta_{ij}) \sum_{l''m''} i^{l-l'-l''} (-1)^{m'+m''} h_{l''}^{(1)}(k|\mathbf{r}_j - \mathbf{r}_i|) Y_{l''-m''}(\mathbf{r}_j \triangleq \mathbf{r}_i) \int Y_{lm} Y_{l''m''} Y_{l'-m'} d\Omega \tag{11}$$

is a propagator from atom i of position vector $\mathbf{r}_i$ to atom j of position vector $\mathbf{r}_j$ in the qth shell. $\tilde{g}_{LL'}^{ij}$ is the same as $g_{LL'}^{ij}$ except that $j_{l''}$ is substituted for $h_{l''}^{(1)}$. The superscript o in the propagators represents the central emitter atom.

The intrashell multiple scattering is represented by the elements $T_{L_iL_j}^{ij}$ of the matrix

$$\mathbf{T} = \mathbf{H}^{-1} , \tag{12}$$

where

$$H^{ij}_{L_iL_j} = t^{(i)-1}_{L_i}\delta_{ij}\delta_{L_iL_j} - g^{ij}_{L_iL_j} \tag{13}$$

are the elements of the real-space Korringa-Kohn-Rostoker (KKR) matrix $\mathbf{H}$ and $t^{(i)}_{L_i}$ is an element of the (diagonal) t matrix of atom i.

With $\mathbf{S}^{(N)}$ calculated by this algorithm, making use of the asymptotic expansion of Hankel functions

$$\lim_{z\to\infty} h^{(1)}_{l'}(z) = (-i)^{l'+1}z^{-1}e^{iz} \tag{14}$$

and neglecting some common constant factors, the angular distribution of the far-field intensity of a photoelectron or Kikuchi diffraction pattern can be evaluated from

$$I_p(\mathbf{k}) = \left|\sum_L A^{(0)}_L \sum_{L'} S^{(N)}_{LL'}(-i)^{l'}Y_{L'}(\hat{\mathbf{k}})\right|^2 , \tag{15}$$

where $S^{(N)}_{LL'}$ are the elements of the matrix $\mathbf{S}^{(N)}$. In the evaluation of I_p in (15) we have allowed for the interference between the angular momentum channels L of the emitted electron. The coefficients $A^{(0)}_L$ can be evaluated from the matrix elements of the atomic excitation process, be it photoexcitation (for photoelectron diffraction) or quasielastic scattering of a plane wave (for Kikuchi diffraction).

In the case of Auger emissions the initial-state angular momentum channels are mutually incoherent, and the angular distribution of an Auger diffraction pattern should instead be evaluated from an expression of the form

$$I_A(\mathbf{k}) = \sum_L \left|A^{(0)}_L \sum_{L'} S^{(N)}_{LL'}(-i)^{l'}Y_{L'}(\hat{\mathbf{k}})\right|^2 , \tag{16}$$

where $A^{(0)}_L$ are now related to the matrix elements for Auger transitions.

III. FINITE ANGULAR RESOLUTION

In any experimental apparatus, the electron detector must integrate over some finite solid angle when making an angle-resolved measurement. For the purposes of our argument, and without loss of generality, we may choose a polar axis passing through the center of the detector. Then the experimentally measured intensity $I_{\exp}(\theta,\phi)$ would be related to the theoretical intensity $I_{th}(\theta,\phi)$ by the equation

$$I_{\exp}(0,0) = \int_{\phi=0}^{2\pi}\int_{\theta=0}^{\theta_m} I_{th}(\theta,\phi)\sin\theta\,d\theta\,d\phi , \tag{17}$$

where we have assumed that the analyzer aperture is circular with angular half-width θ_m. From (15) it can be seen that a theoretical photoemission intensity may be written

$$I_{th}(\theta,\phi) = \sum_{L'}\sum_{L''} A^{(N)}_{L'}A^{(N)*}_{L''}(-i)^{l'-l''}Y_{L'}(\theta,\phi)Y^*_{L''}(\theta,\phi)$$

$$= \sum_{L'}\sum_{L''} A^{(N)}_{L'}A^{(N)*}_{L''}(-i)^{l'-l''}$$

$$\times \sum_{l=|l'-l''|}^{l'+l''}\sum_{m=-l}^{l}\langle L''|L'L\rangle Y^*_{lm}(\theta,\phi) , \tag{18}$$

where

$$A^{(N)}_L = \sum_{L'} A^{(0)}_{L'}S^{(N)}_{L'L} \tag{19}$$

and

$$\langle L''|L'L\rangle = \int Y^*_{L''}Y_{L'}Y_L d\Omega , \tag{20}$$

a Clebsch-Gordon coefficient. Substituting (18) into (17) and performing the integrals over θ and ϕ, we find

$$I_{\exp}(0,0) = 2\pi\sum_{l'}\sum_{l''}(-i)^{l'-l''}\sum_{m'}A^{(N)}_{l'm'}A^{(N)*}_{l''m'}\sum_{l=|l'-l''|}^{l'+l''}\langle l''m'|l'm';l0\rangle\left[\frac{2l+1}{4\pi}\right]^{1/2}Q_l , \tag{21}$$

where

$$Q_l = -\int_1^{\cos\theta_m} P_l(\cos\theta)d(\cos\theta) . \tag{22}$$

Noting that the Legendre function $P_l(z)$ may be represented by the hypergeometric function $F(-l,l+1,1;(1-z)/z)$, substituting its series expansion into (22), and performing the integral over $\cos\theta$ yields

$$Q_l = \xi + \frac{(-l)(l+1)}{(1!)^2 2}\left[\frac{\xi^2}{2}\right] + \frac{(-l)(-l+1)(l+1)(l+2)}{(2!)^2 2^2}\left[\frac{\xi^3}{3}\right] + \cdots$$

$$+ \frac{(-l)(-l+1)\cdots(-l+n-1)(l+1)(l+2)\cdots(l+n)}{(n!)^2 2^n}\left[\frac{\xi^n}{n}\right] + \cdots , \tag{23}$$

where

$$\xi = 1 - \cos(\theta_m) . \tag{24}$$

The quantity Q_l may be evaluated numerically from

the series expansion (23) for different aperture sizes as specified by θ_m. The results are shown in Fig. 1. It will be noted that Q_l drops off with increasing l, and the more sharply the larger the aperture size. In fact, for a typical experimental aperture semiangle of $\theta_m = 2.5°$, Fig. 1 indi-
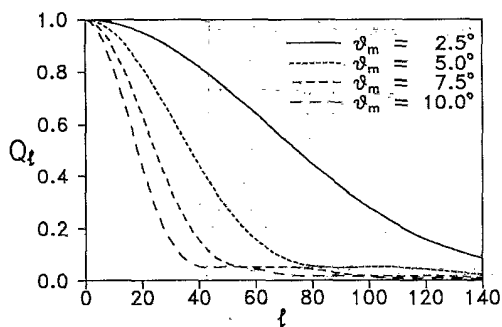
FIG. 1. Theoretical relative contributions, Q_l of angular momenta to an experimental photoelectron diffraction pattern for different half-angles θ_m of the detector aperture.

cates that the contributions of the terms in (21) with values of l greater than about 120 are likely to be negligible. Note that the maximum value of l in the sum in (21) is $l'+l''$ ($=l_m$, say). For a given value of l_m, l' can take values between 0 and l_m, while l'' correspondingly varies from l_m to 0. However, since the lower limit of the sum over l in (21) is $|l'-l''|$, it is clear that the number of allowed terms in the sum over l is greatest when $l' \simeq l'' \simeq l_m/2$. That is, for the highest appreciable value of $l_m \simeq 120$, the most significant contributions to I_{exp} will come from terms with $l' \simeq l'' \simeq 60$. For lower values of l_m the dominant terms will have even lower values of l' and l''. Thus, it may be concluded that an experimental diffraction pattern, measured by a detector of aperture with a semiangle of 2.5°, could be simulated with reasonable accuracy by restricting the angular momentum quantum numbers of the single-center expansions (15) and (16) to

$$l', l'' < l_{\text{out}} \simeq 60 . \tag{25}$$

This conclusion is supported by our test simulations of Sec. V, and by comparisons with experimental diffraction patterns (see, e.g., Fig. 8, and the discussion in Sec. VIII).

It should be noted also that a mere truncation of the angular momentum expansion at $l', l'' = l_{\text{out}}$ is not sufficient to reproduce a finite experimental angular resolution in a calculated diffraction pattern. The reason is found in the gradual decrease of Q_l with l, as seen in Fig. 1. The corresponding gradual attenuation of the spherical-wave amplitudes $A_L^{(N)}$ is not accounted for by just a sharp cutoff at $l = l_{\text{out}}$. The theoretical diffraction patterns also need to be convolved with an aperture function representing the detector. In Sec. V we confirm these conclusions with some test calculations.

IV. THE FORWARD-SCATTERING APPROXIMATION

For subsurface emitters a very convenient approximation to the full multiple-scattering scheme of Sec. II may be found. This takes advantage of the unique geometry of the concentric shells, yields calculated diffraction patterns practically indistinguishable from those from a full multiple-scattering calculation, and affords about an order of magnitude speed-up of the calculation.

The approximation is based on the fact that when a medium-energy electron is incident upon an atom, it is most likely to be scattered with a small angle close to the direction of its initial path, as is now well attested to in numerous publications, e.g., Refs. 17 and 32. It is possible to exploit this forward-scattering behavior in the concentric-shell algorithm (CSA) in two ways: (1) by the neglect of intrashell multiple scattering, and (2) by the successive transmission approximation to intershell multiple scattering. The successive transmission approximation assumes that an outward traveling spherical wave incident on an atomic shell has a negligible backward scattered (i.e., inward traveling) component.

Intrashell multiple scattering can be turned off by neglecting the intrashell propagators $g_{L_i L_j}^{ij}$ in (13) above. This is equivalent to making the approximation

$$T_{L_i L_j}^{ij} \approx t_{L_i}^{(i)} \delta_{ij} \delta_{L_i L_j} \tag{26}$$

in Eqs. (7)–(10).

The inclusion of only forward scattering in the intershell multiple scattering is accomplished by setting the out-in scattering matrices, $\mathbf{T}_q^{OI}$, equal to zero. Then the scattering matrix of the entire cluster takes on the particularly simple form

$$\mathbf{S}^{(N)} \simeq (\mathbf{I}+\mathbf{T}_0^{OO})(\mathbf{I}+\mathbf{T}_1^{OO}) \cdots (\mathbf{I}+\mathbf{T}_N^{OO}) . \tag{27}$$

Note that both these simplifications, which together we term the forward-scattering approximation, avoid the matrix inversion operations necessary for the evaluation of full multiple scattering [see Eqs. (3), (4), and (12)], thus substantially reducing the computational time requirements. Nevertheless, the forward-scattering approximation includes all single-scattering events and all significant multiple-scattering pathways, particularly those which do not contain scattering angles greater than about 90°.

We demonstrate the validity of this approximation scheme with the calculation of the LVV Auger diffraction pattern from a Cu(001) single crystal. We then use the complete Cu(001) calculation to make predictions about the effects of multiple inequivalent electron emitters on the reliability of reconstructions of holographic images by a Helmholz-Kirchhoff algorithm.[4]

V. TESTS OF CONVERGENCE AND APPROXIMATIONS

We first describe the results of tests performed on model atomic clusters to check the convergence of our calculations with respect to various parameters, and to verify the justification of the approximate schemes we described above.

Quantitative comparisons of diffraction patterns are made using a mean-square difference reliability (R) factor[33]

$$R_2 = \frac{\sum_i [P_i^{(1)} - P_i^{(2)}]^2}{\sum_i [P_i^{(1)}]^2} \tag{28}$$

Of the two diffraction patterns to be compared, the reference pattern $P^{(1)}$ is chosen to be the one which is the better approximation. Based on previous results,[33] we expect that $R_2 \sim 0.1$ is the minimum R factor to be expected for the comparison between calculations and experiment. We therefore assume that any approximation which changes the calculated diffraction pattern such that the R factor is less than or equal to $R_2 = 0.001$ is a more than adequate approximation.

All the calculations in this section involve Cu atoms in a geometry corresponding to the face-centered-cubic (fcc) (001) orientation. The electron kinetic energy is 914 eV, which is the energy of the Cu LVV Auger electron. The atomic scattering processes take into account angular momentum quantum numbers up to $l = l_{max} = 15$.[34] All calculations assume an inner potential with real and imaginary parts of -15 and -4 eV, respectively. The zero-temperature phase shifts are corrected by a Debye-Waller factor[35] assuming a Debye temperature of 320 K and a sample temperature of 300 K. Unless otherwise stated, single center expansions are made using angular momentum values up to $l_{out} = 60$, consistent with our argument in Sec. III that this value is adequate for the simulation of diffraction patterns measured with a detector of semiangular aperture of 2.5° angular resolution. In line with this, all calculated diffraction patterns are convolved with a Gaussian angular smoothing function with half-width at half maximum (HWHM) of 2.5°.

We begin by testing our assertions about the adequacy of truncating the angular momentum expansions of our wave fields for finite experimental detector apertures. We present the results of two calculations for the case of a Cu atom emitter in the fourth layer from the surface of a Cu(001) single crystal. In addition to the electron emitter, the atomic cluster contained 238 scattering atoms, with the outermost atomic shell having a radius of 10.6 Å. One calculation, (b), was performed using $l_{out} = 60$, a value large enough for a detector aperture of semiangle 2.5° according to the argument of Sec. III. The other, (a), used $l_{out} = 90$, which should be large enough for a detector of perfect angular resolution.[36] For the reasons explained in Sec. III both patterns were convolved with a Gaussian of angular variance $\sigma = 3°$, representing an experimental angular resolution of 2.5° HWHM. The diffraction patterns from these two calculations are displayed in Fig. 2, and are indistinguishable to the eye. An R-factor comparison of the two patterns results in $R_2 = 0.0004$, which is well within our criterion for a valid approximation.

In order to test the validity of the forward-scattering approximation of Sec. VIII, we performed two calculations, whose results are displayed in Fig. 3. Both computations were for 19-atom clusters of Cu atoms, including an emitter and its first and second nearest neighbors, in the bulk of a Cu crystal. The cluster was oriented with the (001) direction representing the surface normal (pointing towards the center of the diffraction pattern). The calculations assumed an $l = 0$ angular momentum of the emitted electron before scattering, and an electron energy of 914 eV. In Fig. 3, the diffraction pattern labeled (a) utilized the full multiple-scattering algorithm of Sec.
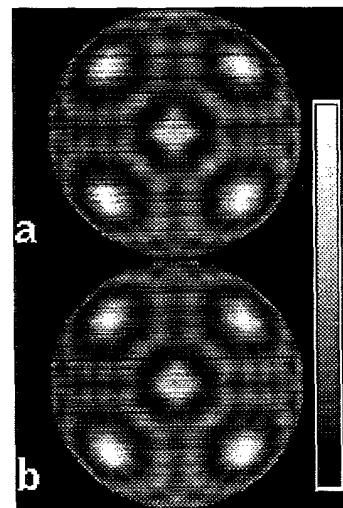

FIG. 2. Comparison of cluster calculations for an emitter atom in the fourth layer from the Cu(001) surface. Pattern (a) uses $l_{max} = 90$, and (b) uses $l_{max} = 60$. Both patterns have been smoothed to simulate a detector of 2.5° aperture semiangle. Pattern (b) appears to be an excellent approximation, since the R factor comparing the two patterns has a value of $R_2 = 0.0004$.

II, and (b) the forward-scattering approximation of Sec. IV. The results of the calculations appear identical to the eye. The R factor relating the two diffraction patterns is as small as $R_2 = 0.000\,09$, demonstrating the excellence of the forward-scattering approximation for such electron kinetic energies.
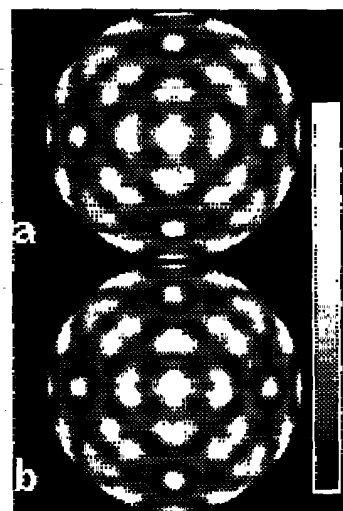

FIG. 3. Comparison of Auger diffraction cluster calculations for 19 Cu atoms in the (001) orientation. Pattern (a) is the result using full multiple scattering and (b) is the result using the forward-scattering approximation. These patterns are virtually identical, with an R factor of $R_2 = 0.000\,09$.

VI. CALCULATED DIFFRACTION PATTERNS DUE TO AUGER EMISSION FROM O ON A Ni(100) SURFACE

As an example of an application of our scheme for the simulation of a realistic experiment, we consider first the diffraction pattern formed by Auger electrons emitted by an O atom adsorbed on the fourfold hollow site on a Ni(100) surface. For simplicity, we assume an s-wave emitter. We take the energy of the emitted electrons to be 504 eV, corresponding to a prominent O Auger line.

Figure 4(a) shows the resulting backscattered diffraction pattern calculated by the full multiple-scattering version of our algorithm for polar angles ranging from zero at the center of the pattern to 70° at the edges. For the purposes of our discussion of the effect of multiple scattering on holographic reconstruction from such a pattern, we show in Fig. 4(b) the corresponding diffraction pattern calculated in the single-scattering (kinematic) limit.

The latter pattern is also calculated by our algorithm, but with the intrashell multiple scattering switched off as described in Sec. IV, and intershell multiple scattering also turned off. The latter is achieved by neglecting the backscattering matrix product $T^{OI}_{q+1}J^{IO}_q$ as in the forward-scattering approximation of Sec. IV, but now additionally only the terms up to first order in the forward-scattering matrices T^{OO}_q in (3) are retained. Then $S^{(N)}$ may be further approximated by

(a)

(b)

FIG. 4. Calculated diffraction patterns for KVV Auger emission from an oxygen atom adsorbed on the fourfold hollow site of a Ni(100) surface, using (a) full multiple scattering, and (b) single scattering. Note that there are significant differences between these two patterns, indicating the necessity of including full multiple scattering for atoms in this geometry.

$$S^{(N)} \simeq I + T^{OO}_1 + T^{OO}_2 + \cdots + T^{OO}_N . \qquad (29)$$

The two diffraction patterns of Fig. 4 show significant differences, demonstrating the importance of multiple scattering in calculations of backscattered diffraction patterns.

VII. HOLOGRAPHIC RECONSTRUCTION OF RELATIVE ATOM POSITIONS: THE EFFECT OF MULTIPLE SCATTERING

In the past few years, the intriguing possibility has been considered of reconstructing the three-dimensional configuration of the scattering atoms nearest the emitter by the direct application of a holographic reconstruction algorithm to the intensity distribution of such a diffraction pattern due to a point source of electrons. For adsorbate emitters, striking reconstructed images have been demonstrated from computer-simulated diffraction patterns by, e.g., Barton[4] and Saldin and co-workers,[5,37] and the effectiveness of this technique in such configurations is now well established. Therefore, in what follows we reconstruct holographic images from our diffraction patterns, partly to confirm the correctness of our simulation of the diffraction pattern, but also to examine and comment on a much-debated topic, namely the effect of multiple scattering on the holographic process.

We perform the holographic reconstruction by means of Barton's algorithm[4]

$$A(x,y,z) = \int I(k_x, k_y) \exp[-i\sqrt{(k^2 - k_x^2 - k_y^2)}z]$$
$$\times e^{-i(k_x x + k_y y)} dk_x dk_y \qquad (30)$$

which relates the amplitude of a reconstructed "image" at a real-space position with Cartesian coordinates (x,y,z) relative to the electron emitter, to the intensities $I(k_x, k_y)$ of a diffraction pattern, where k_x and k_y are the Cartesian components of the local wave vector k of the detected electrons. The corresponding real-space intensity is taken to be $I_{\text{rec}}(x,y,z) = |A(x,y,z)|^2$.

Figure 5 shows a model of the atomic geometry assumed in our calculations of the diffraction pattern. An O atom (hatched circle) is assumed to be adsorbed on a fourfold hollow site of a Ni(100) surface. The light circles represent the positions of the Ni atoms. Figure 6 displays
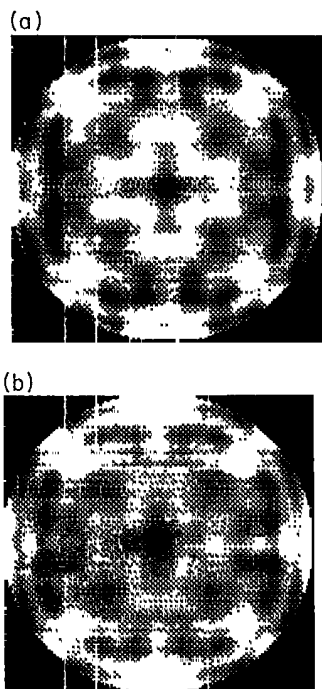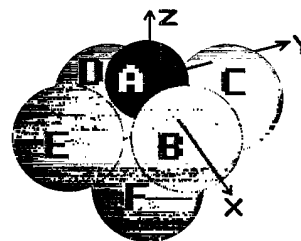
FIG. 5. Model of the atomic geometry used in the calculations of O/Ni(001). The hatched circle represents an O atom adsorbed on a fourfold hollow site of a Ni(100) surface. The light circles represent the positions of the Ni atoms.
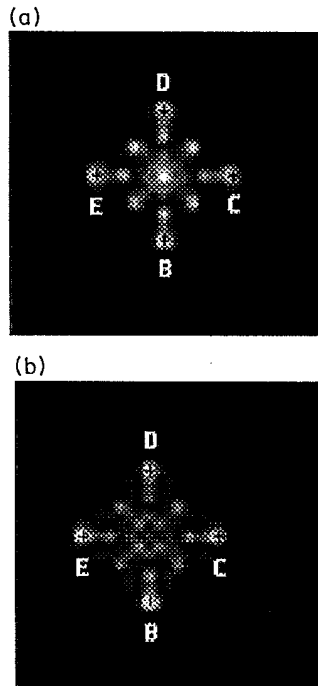
(a)

(b)

FIG. 6. Holographic images obtained from the diffraction patterns in the previous figure, displaying a section through the centers of the nickel atoms at the surface. Image (a) was reconstructed from the multiple-scattering diffraction pattern and (b) from the single-scattering diffraction pattern. Both images show bright features near the positions of substrate atoms.
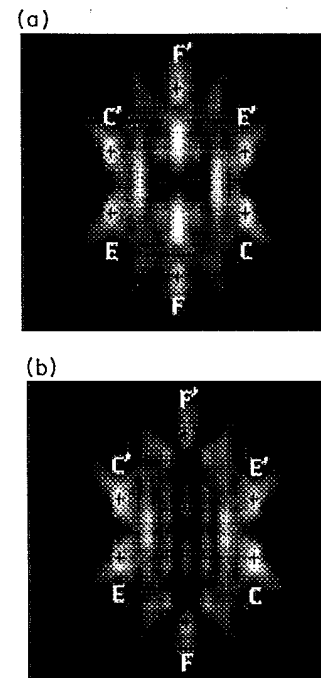
(a)

(b)

FIG. 7. Holographic images obtained as in the previous figure, except that the image sections are oriented perpendicular to the substrate surface, passing through two of the nickel atoms in nearest-neighbor positions with respect to the oxygen atom. Again, both the single-scattering and multiple-scattering diffraction patterns give rise to images of comparable quality.

the variation $I_{rec}(x,y,z=-0.82$ Å$)$ of the reconstructed intensity in the plane of the uppermost layer of Ni atoms on our surface. Part (a) of this figure shows the reconstructed image from the full multiple-scattering diffraction pattern of Fig. 4(a), while part (b) shows that from the single-scattering pattern of Fig. 4(b). Bright spots are seen very close to the positions of the substrate atoms A, B, C, and D of our model, on both parts of the figure. Figures 7(a) and 7(b) depict the corresponding intensities $I_{rec}(x=0,y,z)$ in a plane perpendicular to the surface and passing through two of the nearest-neighbor Ni atoms. Bright intensity streaks, perpendicular to the surface, are seen passing through the positions of the atoms A and B, as well as through "twin-image" positions, C' and D' of atoms C and D, respectively, on the image reconstructed from the multiple-scattering (a) and single-scattering (b) diffraction patterns.

We find no degradation of the reconstructed image due to multiple scattering, despite the noticeable differences between the multiple- and single-scattering patterns in Figs. 4(a) and 4(b), respectively. This serves to confirm an interesting effect which has been noted before:[37] if reconstruction were performed by a traditional holographic algorithm like (30), multiple scattering can actually have a beneficial effect on the resulting image. The explanation is as follows: it is now well established[37] that a Helmholtz-Kirchhoff algorithm (30) will locate the centers of scattering atoms most precisely if both the

reference and object waves are spherically symmetric (i.e., s waves) about their atom centers. In the so-called "forward-scattering" geometry, if the electron energy is greater than about 500 eV, the forward-peaked atomic scattering factors will ensure that the object waves will be far from spherically symmetric, even if single scattering is dominant. It is this fact which led to the invention of reconstruction algorithms[38–40] which correct for the asymmetry of the atomic scattering factors. However, it should be noted that these schemes assume that the object waves arise from kinematic scattering.

Now consider the effect of multiple scattering. It is clear, for instance by examining the algorithm presented in this paper, that on either a single- or multiple-scattering theory, the total wave field emerging from a surface after scattering by the atoms near the emitter can be written as a sum of spherical waves of various angular momentum character centered on each of the scattering atoms. The effect of multiple scattering (as compared with single scattering) is to redistribute amplitudes among the various spherical waves. Now, the singly scattered waves are very aspherical, partly because the electron wave is incident upon each atom from only one direction. In the multiple-scattering case, electron wave amplitude is scattered toward a particular atom from all its atomic neighbors. Therefore, it might be argued that multiple scattering could lead to a decrease in the anisotropy of the scattered wave leaving a particular atom.

Thus, it might be argued that when the Helmholtz-Kirchhoff algorithm (30) is used for holographic reconstruction, multiple scattering is more likely to *enhance* rather than detract from the ability to locate the centers of the scattering atoms. The reconstructed images in Figs. 6 and 7 appear to confirm this.

VIII. APPLICATION TO Cu(001): *LVV* AUGER DIFFRACTION

We next demonstrate the accuracy of the medium-energy approximations to our algorithm by a comparison of a calculated *LVV* Auger diffraction pattern for a Cu(001) single-crystal surface with a corresponding experimental pattern. Calculations were performed for Cu atom emitters in the first through fifth layers from the surface, with the largest atom cluster (corresponding to an emitter in the fifth layer) having 746 atoms. The Cu *LVV* Auger electron has an energy of about 914 eV, and its dominant angular momentum on emission is $l = 3$.[33] For Auger-electron emission, it is assumed that the initially emitted electron wave has a spherically symmetric intensity distribution, i.e., all values of the magnetic quantum number, m, are given equal weight.[33]

Figure 8 displays the comparison of the (a) experimental Cu(001) *LVV* Auger diffraction pattern,[41,33] with (b) the $l = 3$ calculation. Visual comparison of the two diffraction patterns shows that the calculation agrees very well with experiment, both in the positions and intensities of the strongest features in the diffraction patterns. *R*-factor comparison of these two patterns results in $R_2 = 0.097$, giving quantitative proof of this very good agreement. In an earlier paper[33] we also demonstrated the excellence of the agreement by comparing polar-angle scans of the diffraction intensities for two inequivalent

FIG. 9. Comparison of the holographic images obtained from the (a) experimental and (b) calculated diffraction patterns of Fig. 8. These images are horizontal sections parallel to the Cu(001) surface and containing the four nearest neighbors above the electron emitter. Both images are qualitatively quite similar, presenting bright features at the expected atom positions (crosses) but also presenting bright features not associated with atom positions, as in the center of each figure. This good agreement of the holographic images is additional evidence of the accuracy of the calculations.

mirror planes of the Cu(001) surface.

Unlike the preceding section, here the electron emitters are in or below the sample surface. Nevertheless, it has been established experimentally that in this geometry, holographic reconstructions produce images with bright features at atomic positions, for electrons excited by photoemission,[12] Auger,[9] or Kikuchi[8] processes. We can use such holographic images as another way of comparing theory and experiment. Figure 9 shows those reconstructed using Barton's[4] reconstruction algorithm (30) from (a) the experimental diffraction pattern of Fig. 8 and (b) the corresponding simulated pattern. Shown in Fig. 9 are horizontal sections through the three-dimensional reconstructions in a plane parallel to the Cu(001) surface, and one interatomic layer distance above an emitter atom. We see in this figure bright spots at the positions of the Cu atoms in this plane closest to the emitter atom in the layer below. Here again, we find that the agreement of experiment, (a), and calculation, (b), is very good. Both sections show bright features at the positions of nearest-neighbor atoms, which are marked by crosses. But in addition to these features, the calculation also reproduces those features *not* associated with atomic positions, such as the large bright feature at the center.
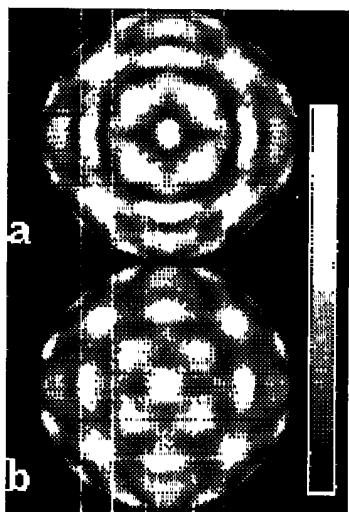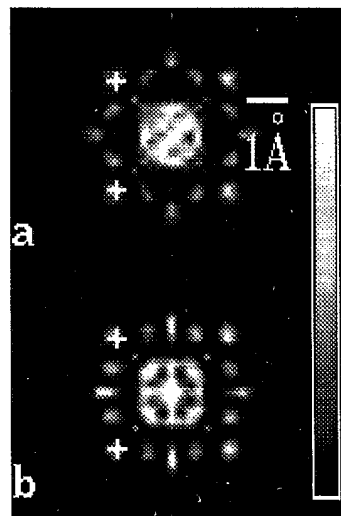

FIG. 8. Comparison of (a) experimental and (b) calculated 914-eV *LVV* Auger diffraction pattern for Cu(001). Good agreement is achieved between experiment and theory, with an *R* factor of $R_2 = 0.097$.

IX. HOLOGRAPHIC RECONSTRUCTION: EFFECT OF EMITTER POSITION

One of the benefits of calculations such as these is that they may be decomposed in a way which is impossible in

an experiment. As an example, we make a study of the effect of the electron emitter position on the holographic reconstruction, when emitters are present simultaneously in many different atomic layers.

In this section a comparison is made of four calculated diffraction patterns due to electron emitters in the first two, three, four, and five layers of a Cu(001) single crystal, and the reconstructed images obtained from each one in turn. The diffraction patterns simulate those which would be observed during the growth of Cu(001) onto a lattice-matched substrate.[42] The five-layer diffraction pattern is essentially converged to that of bulk Cu(001), and was used in Sec. VIII for comparison with the experimental diffraction pattern of bulk Cu. The reconstructed images were calculated in the same way as above and correspond to the same horizontal atomic plane as discussed in Sec. VIII.

Beginning with the two-layer diffraction pattern, Fig. 10(a), four strong forward-scattering features are present at 45° polar angle, and are due to the four nearest-neighbor atoms which reside above the second-layer Cu atoms. These four atoms are clearly visible on the associated reconstructed image displayed in Fig. 11(a). The expected positions of these atoms are displayed in this figure with black crosses, and strong image features at these positions show good agreement with expectation.

The three-layer diffraction pattern, Fig. 10(b), is more complex, presenting all the features of the two-layer pattern, with additional features at normal emission, at about 35° polar angle, and elsewhere. These new
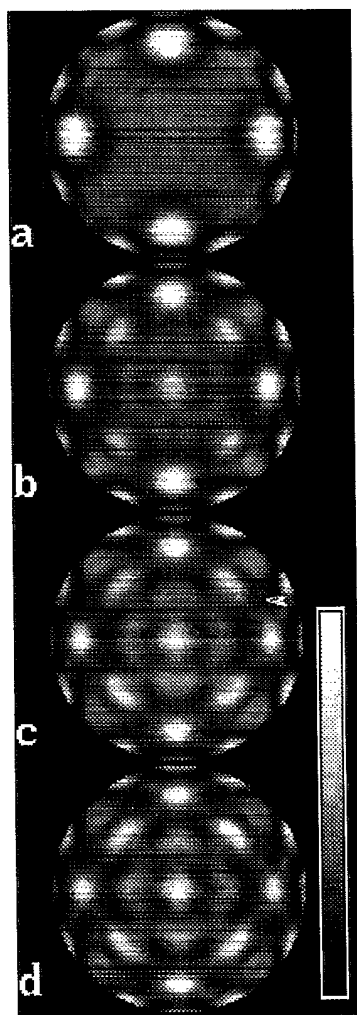

FIG. 10. Calculated diffraction patterns for Cu atoms limited to the first two, three, four, and five atomic layers of a Cu(001) single crystal, labeled (a), (b), (c), and (d), respectively. The diffraction patterns are seen to increase in complexity as layers are added. These patterns simulate the expected behavior of the photoelectron diffraction pattern during film growth of Cu(001) on a lattice-matched substrate.
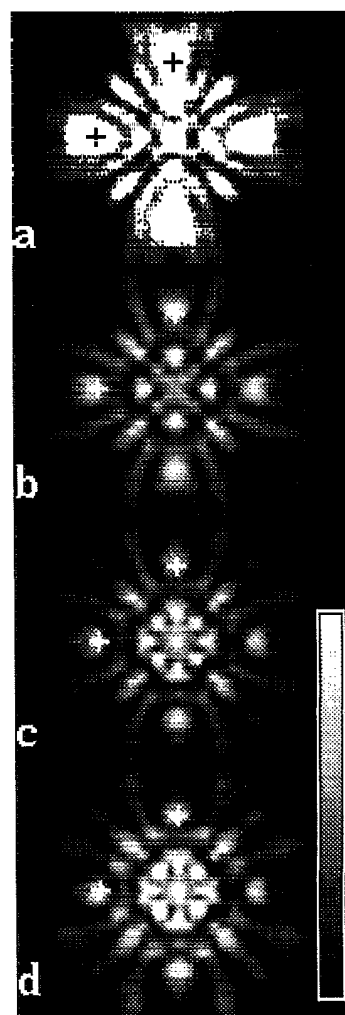

FIG. 11. Holographic images obtained from the diffraction patterns of the previous figure, for 2-, 3-, 4-, and 5-ML Cu films, labeled (a), (b), (c), and (d), respectively. It is seen that the calculations having electron emitters situated farther below the surface (thicker films) give rise to holographic images that are more difficult to interpret. All images show bright features in atom positions, and for thinner films (2–3 ML), these features dominate the image. For thicker films (4–5 ML), spurious nonatomic features make identification of the atomic features more difficult.

forward-scattering features are due to second, third, fourth, etc., nearest-neighbor atoms in the crystal. Ideally, these new diffraction features should have no effect on the holographic image of the nearest-neighbor atoms displayed in Fig. 11(b). Study of the associated image shows that strong features still occur near the expected atomic positions (now denoted by white crosses). However, nonatomic artifacts in the background of the image appear to be increasing in intensity, making the identification of the true atom positons more difficult. This effect is now well understood as being due to the strongly forward-peaked nature of the electron wave as it is scattered by an atom at these energies.[43-46]

The four- and five-layer diffraction patterns/images follow this same trend [Figs. 10, 11(c) and 11(d)]. Thus, even for Cu atoms in the first five layers, bright features can be seen in the positions of nearest-neighbor atoms in the holographic images obtained from the Auger diffraction pattern. But equally strong nonatomic features can also be seen in the background of this image. As mentioned above, these background features are real effects, and are observed (Fig. 9) in the holographic image obtained from an experimental diffraction pattern.

These results make it clear that a Helmholtz-Kirchhoff algorithm, like that originally proposed by Barton,[4] is likely to give rise to good reconstructed images from this type of diffraction pattern due to subsurface emitters only if the emitter lies very close (i.e., in the first to the third atomic layer from the surface). A more sophisticated reconstruction algorithm has been developed,[39] which overcomes some of these distorting effects by compensating for the scattering factor of an atom at the position of the image point currently being reconstructed. An alternative development due to Tong et al.[38] also attempts to compensate for the strong forward-scattering peaks of other atoms at *known* directions from the emitter by dividing by a function containing their scattering factors. It should also be noted that, very recently, a reconstruction algorithm[40] has been demonstrated which offers the prospect of compensating for the effects of all forward-scattering peaks *without a prior knowledge of the positions of any of the atoms.*

X. CONCLUSIONS

We have described an algorithm for the calculation of the angular distributions of Auger, photoelectron, and Kikuchi diffraction patterns which is capable of including *exactly* the multiple scattering of the emitted electrons by a cluster of atoms surrounding the emitter. The size of the cluster is chosen to include all scattering paths which make a significant contribution to the diffraction pattern. The central quantity calculated is the single-center transmission matrix $\mathbf{S}$ of the cluster in an angular

momentum basis. Once calculated, the angular variation of the diffraction pattern may be computed on an arbitrarily fine angular grid with very little extra expenditure of effort. The same is true of calculating the diffraction patterns from different emitted electron states, a feature which we used to advantage recently[33] in determining the angular momentum state of Auger electrons by using a reliability (R) factor to compare an experimental diffraction pattern with simulated patterns due to various emitted electron states.

Although multiple scattering is calculated exactly by our method, it is very easy to switch it off. We take advantage of this feature to compare single- and multiple-scattering diffraction patterns due to Auger emission from an O atom adsorbed on the fourfold hollow site on a Ni(100) surface. We make use of these patterns to examine the effect of multiple scattering on the holographic reconstruction of the local environment of the O atom.

Several medium-energy approximation schemes to the concentric-shell algorithm are outlined, to aid in the efficient calculation of photoelectron, Auger-electron, and Kikuchi-electron[32] diffraction patterns. These approximations take advantage of the unique geometry used in the CSA, which allows the neglect of (1) the (extremely weak) scattering pathways which involve scattering angles greater than 90°, and (2) the high angular-frequency components of the electron intensity distribution which are experimentally immeasurable. It is shown that these approximations are excellent ones by comparisons of calculations made both with and without these approximations.

With these medium-energy approximations installed into the CSA, we calculate the LVV Auger diffraction pattern for Cu(001), at 914 eV. This calculated diffraction pattern shows as good an agreement as any ever obtained[32] between theory and experiment for this well-studied surface, demonstrating the accuracy of the CSA.

The diffraction patterns arising from 2-, 3-, 4-, and 5-ML Cu(001) films were simulated in turn. The results of applying a Helmholtz-Kirchhoff reconstruction algorithm to these diffraction patterns in turn were examined. The thinner films showed reconstructed images much more indicative of atomic positions.

ACKNOWLEDGMENTS

*Present address: IBM Research Division, Almaden Research Center, 650 Harry Rd., San Jose, CA 95120-6099.
[1]For recent reviews of diffuse electron diffraction, see C. F. Fadley, in *Synchrotron Radiation Research: Advances in Surface Science,* edited by R. Z. Bachrach (Plenum, New York, 1990);

W. F. Egelhoff, Jr., Crit. Rev. Solid State Mater. Sci. **16**, 213 (1990); S. A. Chambers, Adv. Phys. **40**, 357 (1991).
[2]G. R. Harp, S. S. P. Parkin, R. F. C. Farrow, R. F. Marks, M. F. Toney, Q. H. Lam, T. A. Rabedeau, and R. J. Savoy, Phys. Rev. B **47**, 8721 (1993).

[3] A. Szöke, in *Short Wavelength Coherent Radiation: Generation and Applications,* edited by D. J. Attwood, and J. Boker, AIP Conf. Proc. No. 147 (American Institute of Physics, New York, 1986).

[4] J. J. Barton, Phys. Rev. Lett. **61,** 1356 (1988).

[5] D. K. Saldin and P. L. De Andres, Phys. Rev. Lett. **64,** 1270 (1990).

[6] D. Gabor, Nature (London) **161,** 777 (1948).

[7] R. J. Collier, C. B. Burckhardt, and L. H. Lin, *Optical Holography* (Academic, New York, 1971).

[8] G. R. Harp, D. K. Saldin, and B. P. Tonner, Phys. Rev. Lett. **65,** 1012 (1990).

[9] G. R. Harp, D. K. Saldin, and B. P. Tonner, Phys. Rev. B **42,** 9199 (1990).

[10] P. Hu and D. A. King, Nature **353,** 831 (1991).

[11] S. Thevuthasan, R. X. Ynzunza, E. D. Tober, C. S. Fadley, A. P. Kaduwela, and M. A. Van Hove, Phys. Rev. Lett. **70,** 595 (1993).

[12] L. J. Terminello, J. J. Barton, and D. A. Lapiano-Smith, Phys. Rev. Lett. **70,** 599 (1993).

[13] S. Kono, C. S. Fadley, N. F. T. Hall, and Z. Hussain, Phys. Rev. Lett. **41,** 117 (1978).

[14] S. Kono, S. M. Goldberg, N. F. T. Hall, and C. S. Fadley, Phys. Rev. Lett. **41,** 1831 (1978).

[15] L.-G. Petersson, S. Kono, N. F. T. Hall, C. S. Fadley, and J. B. Pendry, Phys. Rev. Lett. **42,** 1545 (1979).

[16] H. C. Poon and S. Y. Tong, Phys. Rev. B **30,** 6211 (1984).

[17] S. Y. Tong, H. C. Poon, and D. R. Snider, Phys. Rev. B **32,** 2096 (1985).

[18] P. J. Durham, J. B. Pendry, and C. H. Hodges, Comput. Phys. Commun. **29,** 193 (1982).

[19] D. D. Vvedensky, D. K. Saldin, and J. B. Pendry, Comput. Phys. Commun. **40,** 421 (1986).

[20] J. B. Pendry, in *Determination of Surface Structure by LEED,* edited by P. M. Marcus and F. Jona (Plenum, New York, 1984), p. 3.

[21] D. K. Saldin and J. B. Pendry, Surf. Sci. **162,** 941 (1985).

[22] A. Liebsch, Phys. Rev. Lett. **32,** 1203 (1974).

[23] J. B. Pendry, Surf. Sci. **57,** 679 (1976).

[24] C. H. Li and S. Y. Tong, Phys. Rev. Lett. **40,** 46 (1978).

[25] C. H. Li, A. R. Lubinsky, and S. Y. Tong, Phys. Rev. B **17,** 3128 (1978).

[26] S. Y. Tong and C. H. Li, in *Chemistry and Physics of Solid Surfaces,* edited by R. Vanselow and W. England (CRC, Boca Raton, FL, 1982), Vol. 3, p. 287.

[27] J. J. Barton and D. A. Shirley, Phys. Rev. B **32,** 1906 (1985).

[28] J. J. Barton, M.-L. Xu, and M. A. Van Hove, Phys. Rev. B **37,** 10475 (1988).

[29] V. Fritzsche, J. Phys. Condens. Matter **2,** 1413 (1990); **2,** 9735 (1990).

[30] D. Friedman and C. S. Fadley, J. Electron Spectrosc. Relat. Phenom. **51,** 689 (1990).

[31] J. J. Rehr and R. C. Albers, Phys. Rev. B **41,** 8139 (1990).

[32] G. R. Harp, Ph.D. dissertation, University of Wisconsin–Milwaukee, 1991.

[33] D. K. Saldin, G. R. Harp, and B. P. Tonner, Phys. Rev. B **45,** 9629 (1992).

[34] This parameter was checked for convergence via a calculation involving 13 Cu atoms. An R-factor analysis comparing a calculation with $l_{max} = 15$ and 20 resulted in $R_2 = 0.0004$, showing the computations to be converged to a degree much better than the expected agreement between calculation and experiment.

[35] J. B. Pendry, *Low Energy Electron Diffraction* (Academic, London, 1974), p. 51.

[36] This value of l_{out} should be compared with

$$l_{out} = k r_{max} \qquad (31)$$

suggested by Pendry's (Ref. 35) argument for the number of spherical-wave components needed to represent a wave function of energy $E = k^2/2$ on a shell of radius r_{max}. This would be the value needed for a detector of perfect angular resolution. In the present calculation, $k = 8.2$ a.u.$^{-1}$, and $r_{max} = 20$ a.u., the radius of the atomic cluster. Equation (31) then gives $l_{out} = 164$. Since the calculation time scales approximately as l_{out}^4, criterion (25), which applies to a detector of 2.5° aperture semiangle, leads to a reduction of the computation time by a factor of greater than 50. Note also that the criterion (25) is independent of the electron kinetic energy, so that the computational advantage becomes even more favorable as the electron energy increases. For the present calculation, criterion (31) leads to a shorter computational time for any energy greater than 122 eV.

[37] D. K. Saldin, G. R. Harp, B. L. Chen, and B. P. Tonner, Phys. Rev. B **44,** 2480 (1991).

[38] S. Y. Tong, C. M. Wei, T. C. Zhao, H. Huang, and Hua Li, Phys. Rev. Lett. **66,** 60 (1991).

[39] B. P. Tonner, Z.-L. Han, G. R. Harp, and D. K. Saldin, Phys. Rev. B **43,** 14423 (1991).

[40] D. K. Saldin, X. Chen, N. C. Kothari, and M. H. Patel, Phys. Rev. Lett. **70,** 1112 (1993).

[41] Z.-L. Han, S. Hardcastle, G. R. Harp, H. Li, X.-D. Wang, J. Zhang, and B. P. Tonner, Surf. Sci. **245,** L190 (1991).

[42] In particular, the Cu film growth could be onto a Ni(001) single crystal. This is, in fact, an excellent approximation, because (1) the scattering of electrons from Ni and Cu atoms at these energies is nearly identical, and (2) because electrons scattered from the Ni substrate must undergo large-angle scattering if they are to reach the detector. Since electron scattering at large angles is extremely weak at these kinetic energies, such substrate scattering will contribute negligible intensity to the final diffraction pattern.

[43] Z.-L. Han, S. Hardcastle, G. R. Harp, H. Li, X.-D. Wang, J. Zhang, and B. P. Tonner, Surf. Sci. **258,** 313 (1991).

[44] G. R. Harp, D. K. Saldin, X. Chen, Z.-L. Han, and B. P. Tonner, J. Electron Spectrosc. Relat. Phenom. **57,** 331 (1991).

[45] A. Stuck, D. Naumovic, H. A. Aebischer, T. Greber, J. Osterwalder, and L. Schlapbach, Surf. Sci. **264,** 380 (1992).

[46] A. Stuck, D. Naumovic, T. Greber, J. Osterwalder, and L. Schlapbach, Surf. Sci. **274,** 441 (1992).